Diffraction-free beams with elliptic Bessel envelope in periodic media

Juan J. Miret[1] and Carlos J. Zapata-Rodríguez[2,*]

[1]*Departamento de Óptica, Universidad de Alicante, P. O. Box 99, Alicante, Spain*
[2]*Departamento de Óptica, Universidad de Valencia, Dr. Moliner 50, 46100 Burjassot, Spain*
[*]*Corresponding author: carlos.zapata@uv.es*

Received September 21, 2007; accepted October 14, 2007;
posted November 5, 2007 (Doc. ID 87706); published December 11, 2007

We report on discrete, nondiffracting, paraxial beams with a Bessel spatial envelope in 1D periodic structures of dielectric media. Anisotropy of the envelope profile is demonstrated to behave in the same manner as extraordinary waves in uniaxial crystals. © 2007 Optical Society of America

OCIS codes: 050.0050, 130.2790, 260.1180.

1. INTRODUCTION

Physical mechanisms of light confinement and localization are extensively investigated in the literature. Nonlinear Kerr effect may drive intense-field filamentation, especially in homogeneous [1,2] and periodic structures [3,4], where media are unable to bound an optical wave. Bessel beams constitute a different sort of diffraction-free localized field induced by rephasing [5,6]. The spatial-spectrum constituents of a Bessel beam are phase-matched exclusively at the optic axis, where a high intensity is reached. In vacuum, these spectral constituents are confined along a circumference in the reciprocal space, supporting a radially symmetric field distribution [7,8]. Nondiffracting solutions with azimuthal symmetry are also observed in homogeneous [9] and layered media [10]. However, such a symmetry disappears necessarily in 2D and 3D photonic crystals [11–15], resulting in more complicated patterns.

On the other hand, anisotropic diffraction-free propagation of localized Bessel beams has been reported previously in uniaxial crystals [16], where eccentricity of the elliptic transverse patterns depends upon the refractive indices associated with the ordinary and the extraordinary axes. In this paper we demonstrate the existence of nondiffracting transverse-electric (TE) fields in 1D photonic crystals with spatial localization of elliptic geometry. Contrarily, TE divergenceless fields in dielectric materials considered optically uniaxial correspond to ordinary waves, giving rise to Bessel beams with transverse radial symmetry.

The paper is organized as follows. In Section 2 the basic grounds of diffraction-free wave propagation in a 1D photonic crystal are reviewed. In Section 3 the paraxial approximation is introduced in order to obtain semianalytical expressions of the dispersion surface equation. In Section 4 we investigate the influence of the elliptic geometry of the isofrequency curves over the spatial distribution of a paraxial nondiffracting beam. In Section 5, dispersion curves and wave patterns of localized diffraction-free fields in a layered medium are numerically evaluated and compared with the analytical expressions presented in previous sections. Finally, in Section 6, the main conclusions are outlined.

2. DIFFRACTION-FREE PROPAGATION IN ONE-DIMENSIONAL PHOTONIC CRYSTALS

A 1D periodic dielectric medium may be characterized by a refractive index $n(y)$ and a period L, in such a way that $n(y+L)=n(y)$. In this case, TE fields ($E_y=0$) satisfy $\nabla\mathbf{E}=0$. Assuming a harmonic time dependence $\exp(-i\omega t)$, TE waves propagating in the nonuniform medium are solutions of the Helmholtz wave equation,

$$\nabla^2\mathbf{E} + k_0^2 n^2(y)\mathbf{E} = 0, \tag{1}$$

where $k_0=\omega/c$ is the wavenumber and c is the phase velocity in vacuum. Typically, a TE field is expressed as a superposition of Bloch modes written in the form

$$\mathbf{E}_0 F_{\mathbf{k}}(y)\exp(i\mathbf{kr}), \tag{2}$$

where $\mathbf{E}_0$ stands for a constant amplitude vector and $F_{\mathbf{k}}(y)$ is a wave function of period L that depends upon the pseudomomentum (PM) $\mathbf{k}=(k_x,k_y,k_z)$. In particular, the orthogonality relation $\mathbf{kE}_0=0$ holds for our solenoidal wave fields. The component of the vector $\mathbf{E}_0$ along the z axis is proportional to its component along the x direction, hereon called E_0, and hence a scalar approach for the wave field may be employed. At the end, our reduced problem consists in searching for PMs and their associated wave functions $F_{\mathbf{k}}(y)$ being compatible with the Helmholtz wave equation, i.e., satisfying

$$\mathcal{H}F_{\mathbf{k}} = k_{\perp y}^2 F_{\mathbf{k}}. \tag{3}$$

In particular, $k_{\perp y}$ stands for the modulus of the transverse PM $\mathbf{k}_{\perp y}=(k_x,k_z)$, and the operator:

$$\mathcal{H} = \partial_y^2 + 2ik_y\partial_y - (k_y^2 - k_0^2 n^2). \tag{4}$$

Concretely, the dispersion surface gives k_z as a function of the 2D PM $\mathbf{q}=(k_x,k_y)$, so that a TE field may be generally written as

$$E_x(\mathbf{R},z) = \int E_0(\mathbf{q})F_{\mathbf{k}}(y)\exp(ik_z z)\exp(i\mathbf{qR})\mathrm{d}^2\mathbf{q}, \tag{5}$$

where $\mathbf{R}=(x,y)$ is the transverse spatial coordinate.

A factorization of Eq. (5) in the form $\exp(i\gamma z)\tilde{E}_x(\mathbf{R})$ provides a wave field of invariant intensity pattern in transverse planes. For instance, a single Bloch mode with $k_z(\mathbf{q})=\gamma$ for a given transverse PM (k_x,k_y) is of this type of diffraction-free field. In general, a given axial PM γ (also known as propagation constant) is degenerate, containing a continuous number of Bloch modes having a distinct transverse PM $\mathbf{q}$. A superposition of degenerate Bloch modes may be represented by means of a spatial spectrum,

$$E_0(k_x,k_y) = a(k_x,k_y)\delta[\gamma^2 - k_z^2(k_x,k_y)], \tag{6}$$

where δ is the Dirac delta function and $a(\mathbf{q})$ stands for a spectral amplitude distribution. From Eq. (5) we infer that such a modal superposition is also a diffraction-free field.

At this point, we should emphasize that Bloch modes are inherently unlocalized waves due to the periodic character of the wave function $F_{\mathbf{k}}$. However, localization is expected to occur in a superposition of Bloch modes under a phase matching condition, that is, if on-phase interference is produced at a given point $\mathbf{R}_0=(x_0,y_0)$. For nondiffracting solutions of Eq. (5), a sufficient condition is met if the complex argument of $E_0(\mathbf{q})$ equals that of the term $F_{\mathbf{k}}^*(y_0)\exp(-i\mathbf{qR}_0)$. The oscillatory behavior of $\exp(i\mathbf{qR})$ in the integral supports the phase matching condition to be found uniquely at the singular point $\mathbf{R}_0$.

3. ISOFREQUENCY CURVES IN THE PARAXIAL REGIME

By imposing continuity of $F_{\mathbf{k}}(y)$ and its first derivative, nontrivial solutions of Eq. (3) may be given for PMs satisfying the dispersion equation, which symbolically we write $h(k_y,k_{\perp y}^2)=0$. Interestingly, if the periodic wave function $F_{\mathbf{k}}$ is a solution of Eq. (3) for $\mathbf{k}$, its complex conjugate is also a solution for $-\mathbf{k}$, i.e., $F_{-\mathbf{k}}(y)=F_{\mathbf{k}}^*(y)$, so that $h(-k_y,k_{\perp y}^2)=0$. Here we consider paraxial waves around the z axis in such a way that k_z is of a large positive value satisfying $k_z^2 \gg k_x^2$ and $k_z^2 \gg k_y^2$ simultaneously. In particular, let us assume we find an eigenvalue $k_{\perp y}^2=k_m^2$ of Eq. (3) for $k_y=0$, i.e., $h(0,k_m^2)=0$. In the general case of achieving several eigenvalues for $k_y=0$, for convenience we consider k_m to be the largest positive real number. Therefore, paraxial waves have PMs $\mathbf{k}$ distributed in the vicinity of the on-axis PM $\mathbf{k}_m=(0,0,k_m)$. As a consequence, we may express h in power series and write

$$h(k_y,k_{\perp y}^2) \approx Ak_y^2 + B(k_{\perp y}^2 - k_m^2), \tag{7}$$

where $A=2^{-1}\partial^2 h/\partial(k_y)^2$ and $B=\partial h/\partial(k_{\perp y}^2)$, both evaluated at $\mathbf{k}=\mathbf{k}_m$, are real-valued parameters. We point out that $\partial h/\partial(k_y)$ vanishes at $\mathbf{k}_m$ since h is an even function of k_y.

When the quadratic expansion of the function h given in Eq. (7) equals zero, the dispersion equation approaches

$$k_x^2 + \eta^{-2}k_y^2 + k_z^2 = k_m^2. \tag{8}$$

Since k_z reaches a maximum value k_m, $\eta^2=B/A$ is necessarily a positive real number; therefore, this quadric surface corresponds to a spheroid. Equation (8) turns out to coincide with Fresnel's equation of wave normals (also known as index ellipsoid) corresponding to the extraordinary wave in a crystal that is optically uniaxial along the y axis, being $n_e=k_m/k_0$ and $n_o=n_e\eta$ the extraordinary and ordinary refractive indices, respectively [17–19]. Note that, however, divergenceless fields in uniaxial crystals correspond to ordinary waves, which Fresnel's equation represents as a sphere.

Particularly, isofrequency curves represent points in the (k_x,k_y) space corresponding to Bloch PMs $\mathbf{k}$ having an axial component of the same value γ, i.e., $\gamma^2-k_z^2(k_x,k_y)=0$. These diagrams are suitable for the analysis of diffraction-free beams since, as shown in Eq. (6), they are synthesized as a superposition of Bloch modes associated with a given isofrequency curve. Contrary to the case of homogeneous media, where isofrequency curves are circumferences of different radii [7], a significant anisotropy along the periodicity direction is observed. An analytical equation representing isofrequency curves may be derived by substitution of $k_z=\gamma$ into Eq. (8),

$$\left(\frac{k_x}{\nu}\right)^2 + \left(\frac{k_y}{\eta\nu}\right)^2 = 1, \tag{9}$$

giving rise to ellipses of semiminor axis $\nu=(k_m^2-\gamma^2)^{1/2}$, assuming $\eta>1$, and semimajor axis $\nu\eta$.

4. ELLIPTIC BESSEL ENVELOPE

Let us study nondiffracting paraxial beams of propagation constant $\gamma \lesssim k_m$, constructed from the superposition of a uniform distribution of TE Bloch modes. We conveniently normalize the spectrum, $|a(\mathbf{q})|=1$. These particular paraxial waves have a neglecting component of the vector $\mathbf{E}_0$ along the z axis, as inferred from the orthogonality relation $\mathbf{kE}_0=0$. In agreement with Eqs. (6) and (9) we may write

$$E_0(k_x,k_y) = \exp(-iC)\delta(k_x^2 + \eta^{-2}k_y^2 - \nu^2), \tag{10}$$

where $C(\mathbf{k})=\arg[F_{\mathbf{k}}(0)]$ in order to have a phase matching at the origin, $\mathbf{R}_0=(0,0)$.

An important feature to be exploited in our analysis is the fact that, under general conditions, the periodic wave function $F_{\mathbf{k}}$ is fundamentally invariant upon paraxial PMs. In such a case, $F_{\mathbf{k}}$ could be substituted by that corresponding to the PM $\mathbf{k}_m$, namely, $F_{\mathbf{k}_m}$. For this purpose, let us consider

$$\mathcal{H}F_{\mathbf{k}_m} = [2ik_y\partial_y - (k_y^2 - k_m^2)]F_{\mathbf{k}_m}. \tag{11}$$

A sufficient condition of proximity between the wave functions $F_{\mathbf{k}}$ and $F_{\mathbf{k}_m}$ may be established in the form of the inequality $|(k_{\perp y}^2-\mathcal{H})F_{\mathbf{k}_m}| \ll |k_{\perp y}^2 F_{\mathbf{k}_m}|$. This is satisfied if k_y^2

$\ll k_m^2$, a trivial condition for paraxial waves, and simultaneously

$$|2k_y \partial_y F_{\mathbf{k}_m}| \ll k_{\perp y}^2 |F_{\mathbf{k}_m}|, \tag{12}$$

within a period, $0 \leqslant y < L$. Moreover, the function $F_{\mathbf{k}_m}$ has a periodic variation from which we may estimate the predominant harmonic component is $\exp(i2\pi L^{-1}y)$, which holds for well-behaved spatial distributions of the refraction index $n(y)$ and vacuum wavelengths in the order of L (k_m in the order of $2\pi L^{-1}$). Under these circumstances we make use of the approach $|\partial_y F_{\mathbf{k}_m}| \approx k_m |F_{\mathbf{k}_m}|$; thus, Eq. (12) is further simplified as

$$2k_m |k_y| \ll k_x^2 + k_z^2. \tag{13}$$

In the paraxial approximation ($k_{\perp y}^2 \approx k_m^2$), this condition carries essentially to that given above, $|k_y| \ll k_m$.

Our analysis may be simplified without loss of generality if we consider that the phase constant C vanishes at $\mathbf{k} = \mathbf{k}_m$ ($F_{\mathbf{k}_m}$ may be arbitrarily chosen to be a real function). Introduction of Eq. (10) into Eq. (5), and factoring out the stationary elements $F_{\mathbf{k}}(y)\exp(ik_z z)$ in the integral, results in a wave field,

$$E_x(\mathbf{R}, z) = \exp(i\gamma z) F_{\mathbf{k}_m}(y) W(\mathbf{R}), \tag{14}$$

where

$$W(\mathbf{R}) = \int\int \delta(k_x^2 + \eta^{-2}k_y^2 - \nu^2)\exp[i(k_x x + k_y y)]\mathrm{d}k_x \mathrm{d}k_y. \tag{15}$$

Straightforward evaluation of the integral is performed if we employ elliptic coordinates. Therefore, we define

$$(k_x, k_y) = (q\cos\theta, q\eta\sin\theta), \tag{16}$$

$$(x, y) = (R'\cos\phi, R'\eta^{-1}\sin\phi), \tag{17}$$

so that the function $\mathrm{W}(\mathbf{R}) = W'(R')$ is obtained as

$$W'(R') = \eta \int_0^{2\pi} \int_0^{\infty} \delta(q^2 - \nu^2)\exp[iqR'\cos(\theta - \phi)] q \mathrm{d}q \mathrm{d}\theta. \tag{18}$$

Using the equation $\delta(q - \nu) = 2q\,\delta(q^2 - \nu^2)$ we finally write

$$W'(R') = 2^{-1}\eta \int_0^{2\pi} \exp[i\nu R'\cos(\theta - \phi)]\mathrm{d}\theta = \pi\eta J_0(\nu R'), \tag{19}$$

where J_0 is a Bessel function of the first kind. We derive that W' is independent of the coordinate ϕ, thus having elliptic symmetry of eccentricity $\epsilon = \sqrt{1 - \eta^{-2}}$.

The analysis of the function W' provides important features of the electric field E_x. The Bessel function in $W'(R')$ has an absolute maximum at origin ($R' = 0$), the point where the phase matching condition is imposed. Considering that localization of the diffraction function W' is bounded by the first zero of J_0, it results $\nu R' \approx 0.77\pi$. Equivalently, the ellipse,

$$x^2 + \eta^2 y^2 = 0.59\pi^2 \nu^{-2}, \tag{20}$$

encircles a region where rephasing enables the highest intensities of the electric field. Concretely, along the y axis ($x = 0$), the width $\Delta y = 0.77\pi(\eta\nu)^{-1}$ is much higher than $(\eta k_m)^{-1}$. For moderate eccentricities, ηk_m is of the order of $2\pi L^{-1}$, so that $\Delta y \gg L$. Consequently, W' has a slow variation in comparison with the function $F_{\mathbf{k}_m}(y)$, along the periodicity direction.

Going further with this idea, and based on the analytical description of Eq. (14), the electric field E_x is separated into slow and fast spatial components. This sort of analysis is similar to the envelope function approach based on the multiple scale method. [20–22] Concretely, the paraxial E_x propagates along the optic axis at a spatial frequency,

$$\gamma = (k_m^2 - \nu^2)^{1/2} \approx k_m - \frac{\nu^2}{2k_m} \tag{21}$$

having a carrier transverse waveform $F_{\mathbf{k}_m}(y)$ of period L and an elliptic Bessel envelope $J_0(\nu R')$. Specifically, the field envelope $W(\mathbf{R})$, describing the slowly varying part of the wave function, exceptionally replicates the field pattern in the x direction. As previously shown, wave localization induced by the phase matching condition particularly enforces the envelope function to have a maximum complex amplitude at $\mathbf{R}_0$.

5. EXAMPLE: A LAYERED MEDIUM

Let us illustrate our approach with a simple example. We consider a bivalued function $n(y)$ corresponding to a periodic system made of alternating layers of two dielectric media. Specifically, $n(y) = n_1$ for $0 \leqslant y < a$ (region I) and $n(y) = n_2$ for $-b \leqslant y < 0$ (region II), with $L = a + b$ the period of the layered structure. From Eq. (3) we may express $F_{\mathbf{k}}(y)$ as a linear combination of the functions $\exp(-ik_y y)\exp(\pm\alpha y)$ in region I, where

$$\alpha = (k_{\perp y}^2 - k_0^2 n_1^2)^{1/2}. \tag{22}$$

In region II we conveniently employ a superposition of the functions $\exp(-ik_y y)\exp(\pm i\beta y)$, if $n_2 > n_1$, being

$$\beta = (k_0^2 n_2^2 - k_{\perp y}^2)^{1/2}. \tag{23}$$

By imposing continuity of $F_{\mathbf{k}}(y)$ and its first derivative, nontrivial solutions are given if the dispersion equation $\cos(k_y L) = G(k_{\perp y}^2)$ holds, where the function

$$G = \cosh(\alpha a)\cos(\beta b) + \frac{\alpha^2 - \beta^2}{2\alpha\beta}\sinh(\alpha a)\sin(\beta b). \tag{24}$$

The above-mentioned dispersion equation was first derived for the electronic band structure of a 1D crystal performed with the Kronig–Penney model [23]. Finally, the periodic wave function is then written as

$$F_{\mathbf{k}}(y) = \exp(-ik_y y)\{\beta\sinh[\alpha(a - y)] + \exp(ik_y L) \times [\beta\cos(\beta b)\sinh(\alpha y) + \alpha\cosh(\alpha y)\sin(\beta b)]\}, \tag{25a}$$

in region I, and

$$F_{\mathbf{k}}(y) = \exp(-ik_y y)\{\beta\cos(\beta y)\sinh(\alpha a) - \alpha\cosh(\alpha a)\sin(\beta y) + \alpha\exp(ik_y L)\sin[\beta(b+y)]\}, \quad (25b)$$

in region II, where a convenient constant factor may be inserted into Eqs. (25). We point out that, as expected, this wave function is Hermitic in the PM space, $F_{-\mathbf{k}}(y) = F^*_{\mathbf{k}}(y)$.

In Fig. 1(a) we plot the dispersion equation corresponding to a layered structure of period $L=2.3$ μm comprised of dielectric slabs of width $b=1.7$ μm and refractive index $n_2=1.46$ immersed in air ($n_1=1$ and $a=0.6$ μm), evaluated at $k_0=4.05$ μm^{-1}. It is shown that $k_{\perp y}$ is a periodic function of k_y (with a period $2\pi/L=2.73$ μm^{-1}) and has even symmetry about the origin. The modulus of the transverse PM has an upper limit, $k_{\perp y} \leqslant k_m$, where $k_m = 5.75184$ μm^{-1}, appearing as a discrete number of bandgaps (plotted in yellow). In particular, paraxial waves along the z axis have PMs distributed in the vicinity of the on-axis PM $\mathbf{k}_m=(0,0,k_m)$. Figure 1(b) shows a contour plot of the first-band dispersion surface around $\mathbf{k}_m$ that is found at the origin $(k_x,k_y)=(0,0)$. Contour lines (isofrequency curves) are symmetric about the origin, so that they are plotted in the first quadrant. Concretely, for a fixed $k_z=\gamma$, the values of $|k_y|$ in the first Brillouin zone are bounded by $|k^{-1}_{\perp y}(\gamma)|$, where $k^{-1}_{\perp y}$ is the inverse function of $k_{\perp y}$; on the other hand, $|k_x| \leqslant \nu$.

A quadratic paraxial equation representing isofrequency curves of the form of Eq. (9) is derived as follows. Series expansions within the validity of the paraxial regime provide, on the one hand,

$$\cos(k_y L) \approx 1 - k_y^2 L^2/2, \quad (26)$$

and, on the other hand,

$$G \approx 1 + G'_m(k^2_{\perp y} - k^2_m), \quad (27)$$

where G'_m is the first derivative of G evaluated at $\mathbf{k}_m$. Invoking the narrowband approximation, $\Delta k \ll k_m$, where Δk represents the width of the first band, we find that $G'_m = (k_m \Delta k)^{-1}$. In our numerical example, $G'_m = 7.69$ μm^2 and $(k_m\Delta k)^{-1} = 6.86$ μm^2. Finally, the dispersion equation may be reduced as Eq. (9) if

$$\eta = (2G'_m L^{-2})^{1/2}. \quad (28)$$

The resulting quadric surface is a prolate spheroid when $2G'_m > L^2$, in agreement with Fig. 1(b), where $\eta = 1.71$. Therefore, the eccentricity of the ellipses is $\epsilon = 0.810$. Finally, in terms of the extraordinary and ordinary refractive indices, it is found that $n_e = k_m/k_0 = 1.42$ and $n_0 = 2.42$, respectively.

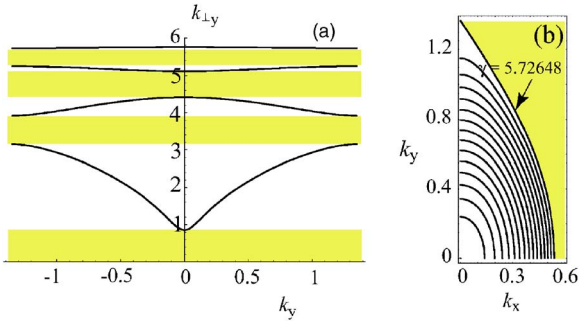

Fig. 1. (Color online) (a) Dispersion equation at vacuum wavelength $\lambda_0 = 1.55$ μm for a layered medium made of dielectric ($n_2 = 1.46$) slabs of width $b = 1.7$ μm immersed in air ($a = 0.6$ μm). (b) Isofrequency curves (only first quadrant) for equidistant values γ of the axial PM belonging to the first band. Bandgaps are plotted in yellow and PMs units are μm^{-1}.

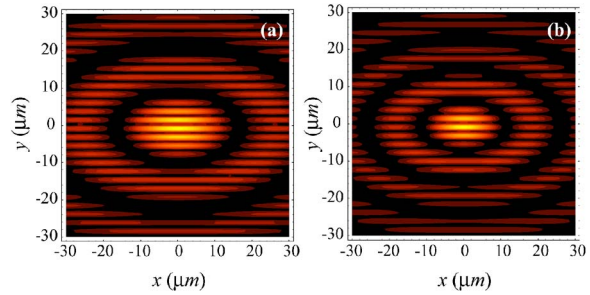

Fig. 2. (Color online) Field strength $|E_x|^2$ in a transverse plane of localized TE waves with a phase matching at $\mathbf{R}_0=(0,0)$ and propagation constant: (a) $\gamma = 5.750$ μm^{-1} ($\nu = 0.145$ μm^{-1}) and (b) $\gamma = 5.748$ μm^{-1} ($\nu = 0.210$ μm^{-1}).

Figure 2 shows the transverse profile of $|E_x|^2$ corresponding to nondiffracting beams of different propagation constants constructed analytically from the superposition of a uniform distribution of TE Bloch modes, as given in Eq. (14). As observed in single Bloch modes, beam depletion in air is produced because of the presence of evanescent waves. As a distinctive feature, light confinement occurs in the dielectric slabs in such a way that the highest intensities are reached at neighboring points of $\mathbf{R}_0 = (0,0)$. In Fig. 2(a), the intensity maximum is not attained at origin but is shifted at $y = -0.849$ μm, approximately at the center of region II. Hence, a focal shift with respect to the wave envelope is observed, which is attributed to the spatial carrier waveform patterning the central lobe. Following the previously given discussion, the origin of these fringes, having a spatial frequency $2\pi/L$ independently of the propagation constant [see also Fig. 2(b)], must be found in the periodic function $F_{\mathbf{k}}(y)$.

Importantly, invariance upon paraxial PMs of the complex periodic function $F_{\mathbf{k}}$ should be guaranteed in order to use the envelope-function approach. Within the spectral regime of validity, $F_{\mathbf{k}}$ is conveniently approximated by

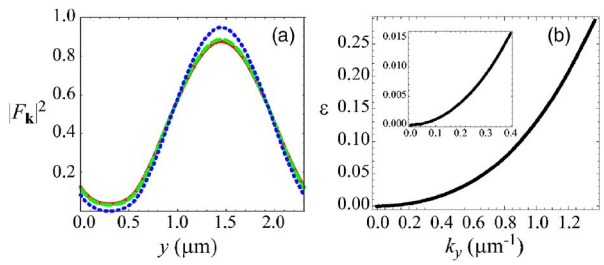

Fig. 3. (Color online) Behavior of the periodic function given in Eq. (25) in the first band. (a) Squared modulus of $F_{\mathbf{k}}$ for different values of k_y; solid curve for $k_y=0$, dashed curve for $k_y = 0.366$ μm^{-1}, and blue dotted curve for $k_y = \pi/L$; and (b) relative error ε versus k_y (inset: ε for $k_y \leqslant 0.4$ μm^{-1}).

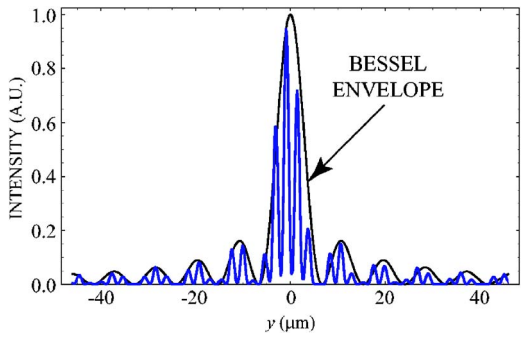

Fig. 4. (Color online) Bessel envelope function $J_0^2(\nu R')$ superposed upon the field intensity $|E_x|^2$, the latter evaluated numerically along the y axis for $\gamma=5.748\ \mu\text{m}^{-1}$.

$F_{\mathbf{k}_m}$, which is a real function. In Fig. 3(a) we show the behavior of $|F_{\mathbf{k}}|^2$ in the first band, for different values of the spectral coordinate $0\leqslant k_y\leqslant \pi L^{-1}$; values of some required parameters are taken from the previous numerical example. For the sake of clarity, we perform a renormalization of the form $\|F_{\mathbf{k}}\|=1$, where

$$\|F_{\mathbf{k}}\| = \int_0^L |F_{\mathbf{k}}(y)|^2 \mathrm{d}y. \tag{29}$$

For the paraxial value $k_y=0.366\ \mu\text{m}^{-1}$, the function $F_{\mathbf{k}}$ does not appreciably change in comparison with the on-axis PM $k_y=0$. Moreover, stationarity of $F_{\mathbf{k}}$ is reassured even for nonparaxial values of k_y; concretely, for the band-edge value $k_y=\pi/L$, the dotted curve of $|F_{\mathbf{k}}|^2$ seems not to deviate in excess from the paraxial lines. In Fig. 3(b) we estimate the relative error $\varepsilon=\|F_{\mathbf{k}}-F_{\mathbf{k}_m}\|$ carried out in the use of the stationary wave function $F_{\mathbf{k}_m}$. We point out that the argument of the normalizing phasor is conveniently introduced in order to minimize ε, where $0\leqslant\varepsilon\leqslant 4$. Specifically for the numerical examples of Fig. 2, we derive that $\varepsilon\leqslant 0.006$ for $\gamma=5.750\ \mu\text{m}^{-1}$, where $|k_y|\leqslant 0.250\ \mu\text{m}^{-1}$, increasing for $\gamma=5.748\ \mu\text{m}^{-1}$ ($|k_y|\leqslant 0.366\ \mu\text{m}^{-1}$) up to $\varepsilon\leqslant 0.013$.

Finally, in Fig. 4, we represent the intensity pattern $|E_x|^2$ derived numerically from Eqs. (5) and (6) for $\gamma=5.748\ \mu\text{m}^{-1}$, together with the slowly varying Bessel envelope $J_0^2(\nu\eta y)$, the former conveniently normalized. The validity of our approach is reconfirmed by explicit comparison of Eq. (14) with our numerical computation [see also Fig. 2(b)], also for long distances far from the origin.

6. CONCLUSIONS

We have presented a particularly interesting spatial distribution of nondiffracting, localized TE waves supported in 1D photonic crystals. The description of the transverse pattern is performed by means of a spatial carrier waveform, directly associated with the Bloch mode for the stationary PM $\mathbf{k}_m$, and a Bessel envelope function of elliptic symmetry that allows a localization of the field. For well-behaved spatial distributions of the refraction index $n(y)$ and vacuum wavelengths in the order of the period L and higher, the envelope function of the paraxial beam carries the slow part of the diffraction pattern, a phenomenon called discrete diffraction [2,24]. Numerical simulations are performed for a layered medium in order to support the validity of our approach. A relevant point to be mentioned is the fact that our analysis may be satisfactorily extended to account for paraxial beam propagation in generic 2D photonic crystals.

ACKNOWLEDGMENTS

This research was funded by the Generalitat Valenciana under project GV/2007/043.

REFERENCES

1. A. Barthelemy, S. Maneuf, and C. Froehly, "Soliton propagation and self-confinement of laser-beams by Kerr optical non-linearity," Opt. Commun. **55**, 201–206 (1985).
2. D. Faccio, A. Averchi, A. Couairon, A. Dubietis, R. Piskarskas, A. Matijosius, F. Bragheri, M. A. Porras, A. Piskarskas, and P. D. Trapani, "Competition between phase-matching and stationarity in Kerr-driven optical pulse filamentation," Phys. Rev. E **74**, 047603 (2006).
3. D. Neshev, E. Ostrovskaya, Y. Kivshar, and W. Krolikowski, "Spatial solitons in optically induced gratings," Opt. Lett. **28**, 710–712 (2003).
4. D. N. Christodoulides, F. Lederer, and Y. Silberberg, "Discretizing light behaviour in linear and nonlinear waveguide lattices," Nature (London) **424**, 817–823 (2003).
5. J. Durnin, "Exact solutions for nondiffracting beams. I. The scalar theory," J. Opt. Soc. Am. A **4**, 651–654 (1987).
6. J. Durnin, J. J. Miceli, and J. H. Eberly, "Diffraction-free beams," Phys. Rev. Lett. **58**, 1499–1501 (1987).
7. G. Indebetouw, "Nondiffracting optical fields: some remarks on their analysis and synthesis," J. Opt. Soc. Am. A **6**, 150–152 (1989).
8. J. Fagerholm, A. T. Friberg, J. Huttunen, D. P. Morgan, and M. M. Salomaa, "Angular-spectrum representation of nondiffracting X waves," Phys. Rev. E **54**, 4347–4352 (1996).
9. M. A. Porras, G. Valiulis, and P. D. Trapani, "Unified description of Bessel X waves with cone dispersion and tilted pulses," Phys. Rev. E **68**, 016613 (2003).
10. S. Longhi, K. Janner, and P. Laporta, "Propagating pulsed Bessel beams in periodic media," J. Opt. B: Quantum Semiclassical Opt. **6**, 477–481 (2004).
11. S. Longhi and D. Janner, "X-shaped waves in photonic crystals," Phys. Rev. B **70**, 235,123 (2004).
12. S. Longhi, "Localized and nonspreading spatiotemporal Wannier wave packets in photonic crystals," Phys. Rev. E **71**, 016603 (2005).
13. O. Manela, M. Segev, and D. N. Christodoulides, "Nondiffracting beams in periodic media," Opt. Lett. **30**, 2611–2613 (2005).
14. K. Staliunas and R. Herrero, "Nondiffractive propagation of light in photonic crystals," Phys. Rev. E **73**, 016601 (2006).
15. J. Hudock, N. K. Efremidis, and D. N. Christodoulides, "Anisotropic diffraction and elliptic discrete solitons in two-dimensional waveguide arrays," Opt. Lett. **29**, 268–270 (2004).
16. A. Ciattoni and C. Palma, "Nondiffracting beams in uniaxial media propagating orthogonally to the optical axis," Opt. Commun. **224**, 175–183 (2003).
17. J. A. Fleck and M. D. Feit, "Beam propagation in uniaxial anisotropic media," J. Opt. Soc. Am. **73**, 920–926 (1983).
18. A. Ciattoni, B. Crosignani, and P. D. Porto, "Vectorial theory of propagation in uniaxially anisotropic media," J. Opt. Soc. Am. A **18**, 1656–1661 (2001).
19. A. Ciattoni and C. Palma, "Optical propagation in uniaxial crystals orthogonal to the optical axis: paraxial theory and beyond," J. Opt. Soc. Am. A **20**, 2163–2170 (2003).
20. J. Sipe and H. Winful, "Nonlinear Schrodinger solitons in a periodic structure," Opt. Lett. **13**, 132–134 (1988).

21. C. M. de Sterke and J. E. Sipe, "Envelope-function approach for the electrodynamics of nonlinear periodic structures," Phys. Rev. A **38**, 5149–5165 (1988).
22. C. M. de Sterke and J. E. Sipe, "Extensions and generalizations of an envelope-function approach for the electrodynamics of nonlinear periodic structures," Phys. Rev. A **39**, 5163–5178 (1989).
23. R. de L. Kronig and W. G. Penney, "Quantum mechanics of electrons in crystal lattices," Proc. R. Soc. London, Ser. A **130**, 499–513 (1931).
24. H. S. Eisenberg, Y. Silberberg, R. Morandotti, and J. S. Aitchison, "Diffraction management," Phys. Rev. Lett. **85**, 1863–1866 (2000).